engineering proceedings

MDPI

Proceeding Paper

Input Shaping for Robust Vibration Suppression in Three Prismatic Joint-Cartesian Robots with Variable *Z*-Axis Dynamics for Automated Optical Inspection †

Demian Escurra [1,*], Luis M. Prieto [1], Luis E. Vázquez [1], Shu-Hao Liang [2] and Marnel Altius [2]

[1] Department of Mechanical Engineering, National Taiwan University of Science and Technology, Taipei City 106335, Taiwan
[2] Graduate Institute of Intelligent Manufacturing Tech, National Taiwan University of Science and Technology, Taipei City 106335, Taiwan; shuhaoliang@mail.ntust.edu.tw (S.-H.L.); d11251801@mail.ntust.edu.tw (M.A.)
* Correspondence: eliazartev84@gmail.com
† Presented at the 6th International Conference on Electronic Communications, Internet of Things and Big Data (ICEIB 2026), New Taipei, Taiwan, 24–26 April 2026.

Abstract

High-speed point-to-point motion in Prismatic–Prismatic–Prismatic (PPP) Cartesian robots used for automated optical inspection (AOI) of printed circuit boards produces residual vibrations. The system must wait until the camera head settles before image capture, which reduces inspection throughput. Input shaping is a common feedforward method for vibration suppression. Its use in reconfigurable Cartesian robots is complicated by workspace-dependent changes in natural frequency along the *Z*-axis and *Y*-axis. To overcome such limitations, we designed and validated a zero-vibration and derivative (ZVD) input shaper implemented on an Espressif Systems Platform 32 microcontroller for a PPP Cartesian AOI robot. The dominant flexible mode of the *X*-axis belt drive was identified experimentally. Accelerometer ring-down data were collected across nine workspace configurations. Frequency was extracted using Fast Fourier Transform, and damping was estimated with logarithmic decrement. The mean natural frequency was 15.34 ± 1.9 Hz, with a damping ratio of 0.032 ± 0.007. A lookup table of ZVD shapers was created for each *Y*-axis position and tested across seven configurations spanning three Z positions and three *Y* positions. The experiments showed RMS residual vibration reductions between 5.3 and 70.7%, with a mean reduction of 43.7% and a maximum peak reduction of 79.1%. Simulation sweeps confirmed that configurations with frequency ratios between 0.6 and 1.4 relative to the design frequency achieved consistent suppression. This provides a practical guideline for workspace-varying systems.

Keywords: input shaping; residual vibration suppression; Cartesian robots; ZVD shaper; time-varying dynamics

Check for updates

Academic Editors: Teen-Hang Meen, Shu-Han Liao and Cheng-Fu Yang

Published: 19 November 2026

Copyright: © 2026 by the authors. Licensee MDPI, Basel, Switzerland. This article is an open access article distributed under the terms and conditions of the Creative Commons Attribution (CC BY) license.

1. Introduction

Automated optical inspection (AOI) of printed circuit boards requires both high positioning accuracy and high throughput. However, in Cartesian robot platforms, these goals conflict. Faster motion reduces cycle time but increases residual vibrations. The system must then wait for the camera head to settle before image capture. This settling time creates dead time and limits throughput, especially in high-mix, low-volume production.

The behavior of belt-driven Cartesian robots is affected by structural flexibility and transmission compliance. The belt drive introduces a resonant mode whose frequency

depends on belt stiffness, cart mass, and motor-side inertia, as described by the two-mass model [1,2]. Rapid trapezoidal commands are used to excite this mode, producing oscillations after each stop. An accelerometer at the camera head is used to measure these vibrations directly. In PPP configurations with a variable-length *Z*-axis, compliance changes with Z-extension, shifting the natural frequency and complicating fixed-parameter suppression.

Input shaping is used in a feedforward method for vibration reduction. The method is used to modify the motion command by convolving it with impulses that cancel residual oscillations [3,4]. The zero vibration and derivative (ZVD) shaper is used to ensure robustness by constraining the derivative of the residual vibration with respect to frequency. This makes it well-suited for systems with uncertain or varying natural frequencies [3]. Input shaping has been validated on Cartesian robots [5].

In this study, we designed and validated a ZVD input shaper for a PPP Cartesian AOI robot. The dominant flexible mode of the *X*-axis belt drive was identified from post-stop ring-down measurements at multiple workspace configurations. A fixed-parameter ZVD shaper was implemented on the robot's microcontroller. Simulation using a second-order model showed near-complete cancellation at the design frequency. Experiments demonstrated that the root mean square of residual vibration reductions ranged between 5.3 and 70.7%, with a mean of 43.7% and a maximum peak reduction of 79.1%. A robustness sweep was used to quantify the effective frequency range. Configurations within a ratio of 0.6–1.4 relative to the design frequency were identified for consistent suppression. This range serves as a guideline for the workspace-varying system.

2. Methodology

2.1. System Description

The experimental platform is a PPP Cartesian robot developed for AOI of PCBs. The *X*- and *Y*-axes each follow the signal chain: Espressif Systems Platform (ESP) 32 microcontroller (Espressif Systems, Shanghai, China) → stepper motor driver → National Electrical Manufacturers Association 17 stepper motor (generic model 17HS8401, obtained from an online retailer; manufacturer not specified) → pulley-belt transmission → linear cart. The *Z*-axis presents a ball-screw mechanism that carries the camera head assembly with the tip mass m_{tip}. A triaxial accelerometer mounted on the camera head records vibration responses during and after positioning moves. The ZVD input shaping algorithm is designed in MATLAB R2024b, and the resulting impulse sequence is deployed on the microcontroller. Real-time command convolution is performed before transmission to the stepper motor drivers.

2.2. System Modeling

The belt-driven *X* and *Y* axes are modeled as a two-mass system consisting of a motor-side equivalent inertia J_e and a cart of mass M, coupled through a compliant belt of effective stiffness K_{eff}. Neglecting pulley inertia and damping, the flexible mode resonance frequency of this system is defined as follows [1,2].

$$f_{\text{res}} = \frac{1}{2\pi}\sqrt{\frac{K_{\text{eff}}(J_e + MR^2)}{J_e M}} \tag{1}$$

where f_{res} is the flexible mode resonance frequency, K_{eff} is the effective belt stiffness, J_e is the motor-side equivalent inertia, M is the cart mass, and R is the pulley radius. This resonance is the dominant flexible mode excited by the trapezoidal motion command and is the target of the ZVD shaper design. For the shaper design, the belt-drive flexible mode is reduced to a single second-order modal model with the experimentally identified natural frequency ω_n and damping ratio ζ. The *Z*-axis arm is modeled as a massless Euler–Bernoulli cantilever

of flexural rigidity EI, where E is the Young's modulus of the material and I is the second moment of area of the cross-section, carrying a concentrated tip mass m_{tip}, following the standard lumped-parameter approximation [1,6]. The natural frequency varies with the *Z*-axis extension z as follows.

$$\omega_{\text{n}}(z) = \sqrt{\frac{3EI}{m_{\text{tip}} \cdot z^3}} \tag{2}$$

where $\omega_{\text{n}}(\text{z})$ is the natural frequency (rad/s) at the Z-axis extension z, related to the frequency in Hz by $\omega_{\text{n}} = 2\pi f_{\text{n}}$ This expression shows that increasing Z extension reduces structural stiffness and shifts the resonant frequency downward, motivating the characterization of f_{n} across multiple Z positions.

2.3. System Identification

The dominant modal parameters of the *X*-axis were identified from post-stop ring-down measurements. Point-to-point moves were executed along the *X*-axis [distance $(D) = 19.2$ cm, velocity $(V) = 30.0$ cm/s, acceleration $(A) = 220.0$ cm/s^2] at three *Y*-axis positions (y = 4.5, 9.5, and 14.5 cm) with the *Z*-axis at its minimum height position (z_{min}, corresponding to maximum arm extension and minimum structural stiffness). After each move, the accelerometer's axial-*z* signal during the post-stop phase was isolated. The steady-state offset was subtracted, and a fourth-order Butterworth low-pass filter with a cutoff frequency of 35 Hz was applied to isolate the structural vibration mode. The natural frequency (f_{n}) was identified from the dominant peak of the Fast Fourier Transform (FFT) of the filtered ring-down signal. The damping ratio (ζ) was estimated using the logarithmic decrement method [3,6].

$$\delta = \frac{1}{N} ln\left(\frac{A_1}{A_{\text{N+1}}}\right), \quad \zeta = \frac{\delta}{\sqrt{(2\pi)^2 + \delta^2}} \tag{3}$$

where A_1 and $A_{\text{N+1}}$ are the amplitudes of the first and (N + 1)-th positive peaks of the ring-down. Three repeated trials were performed at each Y position. The identified parameters, averaged across all nine trials, are $f_{\text{n}} = 15.34 \pm 1.9$ Hz and $\zeta = 0.032 \pm 0.007$. These values served as the design parameters for the ZVD shaper.

2.4. ZVD Shaper Design

Input shaping suppresses residual vibration by convolving the reference command with a sequence of impulses that cancel the system's residual oscillation [5]. The ZVD shaper constrains both the residual vibration amplitude and its derivative with respect to frequency to zero at the design frequency, yielding greater robustness to modeling errors than the two-impulse ZVD shaper [5]. The three-impulse ZVD sequence is given by Singhose [3]. The shaped command is formed as:

$$u_s(t) = \sum_{i=1}^{3} A_i \cdot u(t - T_i) \tag{4}$$

where $u(t)$ is the original trapezoidal position command [4]. The shaper adds T_3 to the total move duration, a small penalty relative to the settling time reduction achieved. A per-*Y*-position lookup table of ZVD shaper coefficients was implemented on the ESP32 microcontroller, selecting the correct shaper automatically on the basis of current *Y*-axis position before each *X*-axis move. Design frequencies were determined empirically from preliminary ring-down tests at each Y position. Table 1 shows the shape coefficients deployed on the robot.

https://doi.org/10.3390/engproc2026159053

Table 1. ZVD shaper parameters deployed per *Y*-axis configuration with varying *X*-axis at z_{min}.

Y Position (cm)	f_n (Hz)	ζ	A_1	A_2	A_3	T_2 (s)	T_3 (s)
14.5	11.1	0.035	0.2782	0.4985	0.2233	0.04507	0.09015
9.5	11.3	0.035	0.2782	0.4985	0.2233	0.04428	0.08855
4.5	11.6	0.035	0.2782	0.4985	0.2233	0.04310	0.08621

Note: f_n and ζ were identified experimentally at each Y position. A_i and T_i correspond to the ZVD shaper coefficients computed for each configuration. z_{min}: Maximum *Z*-axis extension, minimum structural stiffness.

2.5. Simulation Setup

The flexible mode response was simulated using a second-order base-excitation model driven by the trapezoidal acceleration command $\ddot{u}(t)$ [1,3]. The governing equation during the move is defined as;

$$\ddot{x} + 2\zeta\omega_n\dot{x} + \omega_n^2 x = \ddot{u}(t) \quad (5)$$

where x is the relative tip displacement and $\ddot{u}(t)$ is the rigid-body cart acceleration, computed as the second derivative of the trapezoidal position command [3,7]. Initial conditions at the moment of stop, $[x(t_{stop})$ and $\dot{x}(t_{stop})]$, are obtained by integrating Equation (5) over the move duration using MATLAB's ode45 solver. The post-stop free ring-down from these initial conditions is then computed from the homogeneous form of Equation (5) and compared between the unshaped and ZVD-shaped cases. The performance metrics are peak residual acceleration $E_{peak} = \max|\ddot{x}(t)|$ and root mean square (RMS) residual acceleration $E_{rms} = \sqrt{\text{mean}(\ddot{x}^2)}$ computed over the post-stop window.

3. Experiment

Simulation

The second-order base-excitation model described in Section 2.5 was simulated in MATLAB R2024b using ode45 numerical integration. For the unshaped and ZVD-shaped commands, the forced ordinary differential equation was integrated over the trapezoidal move duration (D = 19.2 cm, V = 30.0 cm/s, A = 220.0 cm/s^2) to compute the flexible mode displacement and velocity at the moment of stop. The free ring-down from those initial conditions was then simulated, and the residual acceleration was reconstructed as $\ddot{x}(t) = -\omega_n^2 x - 2\zeta\omega_n\dot{x}$. All simulations used f_n = 11.1 Hz and ζ = 0.035, matching the shaper deployed on the robot for the z_{min}, y = 14.5 cm configuration (Figure 1).

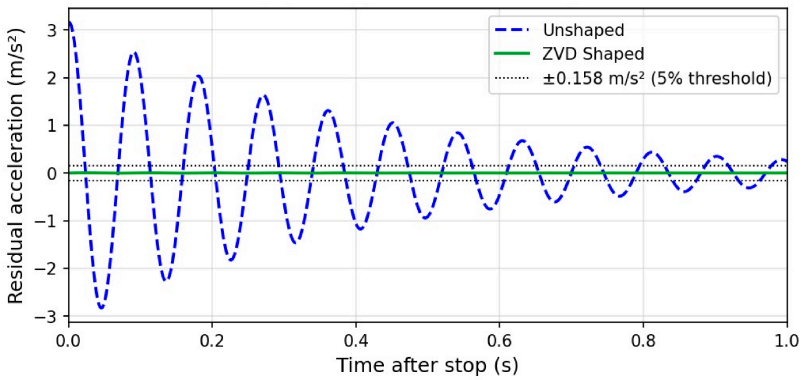


Figure 1. Simulated post-stop ring-down at the ZVD design frequency (f_n = 11.1 Hz, ζ = 0.035). The unshaped command leaves significant residual energy at stop, producing a sustained oscillation. The ZVD-shaped command arrives at the stop with near-zero flexible mode energy, confirming the cancellation mechanism. Dotted lines indicate the ±5% settling threshold.

Point-to-point moves (D = 19.2 cm, V = 30.0 cm/s, A = 220.0 cm/s^2) were executed along the X-axis across seven configurations spanning three Z-axis positions (z_{min}, z_{mid}, z_{max}) and three Y-axis positions (y = 4.5, 9.5, and 14.5 cm), with and without the ZVD shaper. Residual vibrations were recorded using an MPU-6050 triaxial microelectromechanical systems accelerometer (InvenSense, San Jose, CA, USA; module supplier not recorded) at 400 Hz using the ESP32 microcontroller. Three repeated trials were performed per configuration where possible. The post-stop accelerometer signal (phase = 2) was low-pass filtered at 35 Hz, and the residual metrics peak residual acceleration (E_{peak}) and root mean square residual acceleration (E_{rms}) were computed over the first 0.6 s after stop. Figure 2 shows a scatter plot of RMS reduction versus frequency ratio across all seven configurations. The experimental points broadly follow the predicted trend, with higher reductions observed when the ratio is near 1.0 or when the baseline vibration amplitude is large enough for the shaper effect to dominate over measurement noise [5,8].

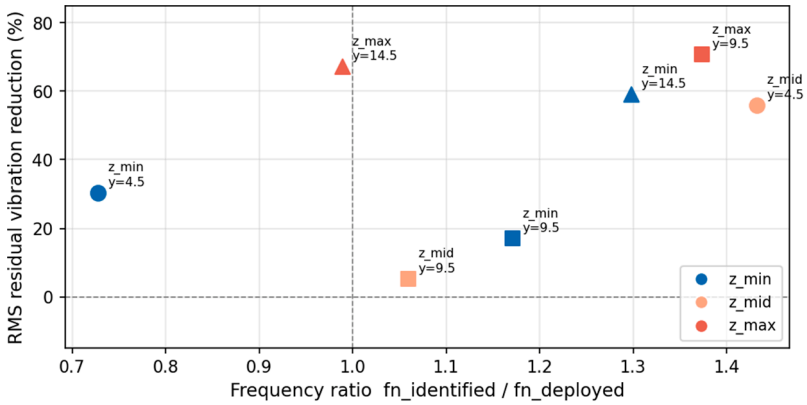


Figure 2. Experimental ZVD scatter plot (RMS residual vibration as percentage of unshaped, normalized to design frequency).

4. Results

4.1. Simulation Results

All simulations used a natural frequency (f_n) of 11.1 Hz and a damping ratio (ζ) of 0.035, matching the shaper deployed on the robot for the z_{min}, y = 14.5 cm configuration. The base-excitation second-order model predicts that the ZVD shaper arrives at the stop moment with near-zero flexible mode energy when the design frequency matches the actual system resonance. Figure 1 shows the simulated post-stop ring-down at the nominal design condition (f_n = 11.1 Hz, ζ = 0.035). The unshaped response produces a damped sinusoid that decays over approximately 0.9 s. The ZVD-shaped response begins near zero, confirming theoretical cancellation of residual energy at the design frequency. The parametric robustness sweep shows that effective suppression extends over a frequency ratio range of about 0.6–1.4. This result is consistent with the known ZVD insensitivity bandwidth [3]. Outside this range, residual vibration increases rapidly.

4.2. Experimental Results

Table 2 shows the measured residual vibration metrics across all seven validated configurations. The RMS of the residual vibration reductions ranged from 5.3 to 70.7%, with a mean reduction of 43.7%. Peak reductions ranged from −4.4 to 79.1%. Settling time at the 5% threshold was reduced by 47.0% in the z_{max}, y = 14.5 cm configuration (from 0.950 s to 0.503 s), which also showed the highest unshaped vibration amplitude in the dataset (E_{peak} = 2.939 m/s^2).

Table 2. Experimental residual vibration reduction—all validated configurations.

Z Position	Y (cm)	f_n Identification (Hz)	f_n Depth (Hz)	Ratio	E_{peak} Unshaped (m/s^2)	E_{peak} Shaped (m/s^2)	Peak Reduction	E_{rms} Unshaped (m/s^2)	E_{rms} Shaped (m/s^2)	RMS Reduction
z_{min}	4.5	8.44	11.6	0.73	0.515	0.265	48.5%	0.161	0.112	30.4%
z_{min}	9.5	13.23	11.3	1.17	0.399	0.416	−4.4%	0.170	0.141	17.0%
z_{min}	14.5	14.41	11.1	1.30	0.906	0.344	62.1%	0.296	0.121	59.1%
z_{mid}	4.5	16.61	11.6	1.43	0.817	0.411	49.8%	0.289	0.127	56.0%
z_{mid}	9.5	11.97	11.3	1.06	0.793	0.775	2.4%	0.286	0.270	5.3%
z_{max}	9.5	15.52	11.3	1.37	0.871	0.196	77.5%	0.250	0.073	70.7%
z_{max}	14.5	10.98	11.1	0.99	2.939	0.614	79.1%	0.599	0.197	67.2%

Note: $f_{n,ident}$ is the identified natural frequency and $f_{n,dep}$ is the deployed (design) frequency used by the shaper. E_{peak} and E_{rms} are the peak and root-mean-square residual accelerations measured over the 0.6 s post-stop window, for the unshaped and ZVD-shaped commands. Peak reduction and RMS reduction are computed as the percentage decrease in E_{peak} and E_{rms}, respectively, between the unshaped and shaped cases: reduction (%) = (unshaped − shaped)/unshaped × 100.

Figure 3 shows the post-stop ring-down at z_{max}, $y = 14.5$ cm, the configuration with the strongest and clearest result. The ZVD-shaped response achieved immediate and sustained reduction from the first oscillation cycle. Peak residual acceleration (E_{peak}) decreased from 2.939 m/s^2 to 0.614 m/s^2 (79.1%), and RMS residual acceleration (E_{rms}) decreased from 0.599 m/s^2 to 0.197 m/s^2 (67.2%). Configurations with frequency ratio $f_{n,identified}/f_{n,deployed}$ between 0.73 and 1.43—covering all tested cases (with 1.43 marginally above the upper edge of the band) —achieved meaningful RMS reductions in five of seven configurations. The two weaker cases (z_{min}, $y = 9.5$ cm: 17.0% RMS; z_{mid}, $y = 9.5$ cm: 5.3% RMS) shared a common feature: low baseline vibration amplitude compared to other configurations. This reduced the signal-to-noise ratio of the MPU-6050 measurement and increased trial-to-trial variability relative to the mean reduction. At z_{min}, $y = 9.5$ cm, the frequency ratio of 1.17 also placed the configuration closer to the edge of the robustness band than the higher-performing cases.

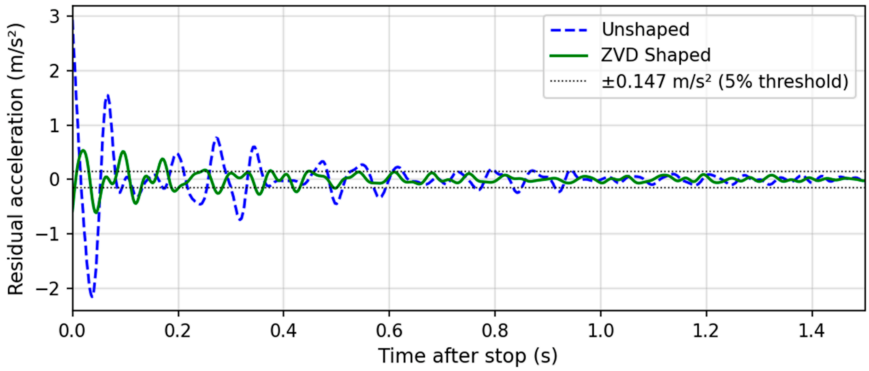


Figure 3. Post-stop residual acceleration at z_{max}, y = 14.5 cm—unshaped (dashed) vs. ZVD-shaped (solid). Dotted lines indicate the ±5% settling threshold.

5. Discussion

ZVD input shaping is an effective feedforward strategy for suppressing residual vibration in a PPP Cartesian robot operating across a variable workspace. A per-Y-position lookup table of ZVD shapers, each designed from empirically identified modal parameters, was implemented on the ESP32 microcontroller and validated across seven configurations spanning three Z positions and three Y positions. The RMS residual vibration reduction of 43.7% was achieved, with individual reductions reaching 70.7% at z_{max}, $y = 9.5$ cm and 67.2% at z_{max}, $y = 14.5$ cm. Settling time at the 5% threshold was reduced by 47.0% in the

highest-amplitude configuration, directly lowering dead time between positioning moves and image acquisition in the AOI cycle.

Variation in shaper effectiveness ranged from near-zero improvement to 71% RMS reduction. Configurations with higher unshaped vibration amplitude produced larger absolute improvements and clearer signal-to-noise ratios for the MPU-6050 accelerometer. The frequency ratio between the actual resonance and the deployed design frequency determined whether the configuration fell within the ZVD robustness band. The experimental scatter plot confirmed that the robustness band predicted by simulation (ratio = 0.6–1.4) matched the boundary between effective and ineffective suppression, validating the second-order base-excitation model as sufficient for shaper design.

A discrepancy was observed between the preliminary design frequencies (11.1–11.6 Hz) and the FFT-based ring-down identification (8.44–16.61 Hz across the workspace). This indicates the difficulty of identifying modal parameters with a low-cost accelerometer under open-loop stepper excitation and highlights sensitivity to signal processing choices. Despite this, the ZVD shaper's robustness to frequency uncertainty ensured effective suppression in most configurations, demonstrating practical feasibility even with imperfect identification.

Several limitations must be addressed. The open-loop stepper motor architecture provides no position feedback, so step losses at high accelerations could introduce errors not captured by the model or detected by the accelerometer. The MPU-6050 accelerometer lacked resolution for reliable results at low-amplitude configurations, reducing accuracy in two cases. The *Z*-axis cantilever model was not experimentally validated due to sensor resolution limits at low vibration levels. First, to overcome the limitations, the MPU-6050 accelerometer must be replaced with higher-resolution inertial sensors or laser displacement systems to enable accurate identification across the full workspace. Second, adaptive shaping strategies must be adopted to update parameters in real time from ring-down measurements and eliminate reliance on preliminary identification and continuously handle workspace-dependent frequency shifts. Third, Full AOI scan trajectories, including combined X and Y moves, must be validated to strengthen applicability to complete inspection cycles.

6. Conclusions

In this study, the design, simulation, and experimental validation of a ZVD input shaper are developed for a PPP Cartesian AOI robot with variable *Z*-axis dynamics. The shaper was implemented on a low-cost ESP32 microcontroller using per-configuration lookup table selection, requiring no additional sensors beyond the onboard accelerometer. The experimental results across seven workspace configurations confirmed residual vibration reductions of up to 79.1% in peak and 70.7% in RMS. These results indicate the practical feasibility of input shaping for throughput improvement in printed circuit board inspection systems.

Author Contributions: Conceptualization, D.E., L.E.V. and L.M.P.; methodology, D.E.; software, L.E.V.; validation, D.E. and L.E.V.; formal analysis, D.E.; investigation, D.E., L.E.V. and L.M.P.; resources, L.M.P.; data curation, L.E.V.; writing—original draft preparation, D.E.; writing—review and editing, D.E., L.E.V. and L.M.P.; visualization, D.E.; supervision, S.-H.L. and M.A.; project administration, D.E.; funding acquisition, S.-H.L. All authors have read and agreed to the published version of the manuscript.

Funding: This research was supported by the Intelligent Manufacturing Innovation Center (NTUST) within the Featured Areas Research Center Program and the Higher Education Sprout Project Framework of the Ministry of Education, Taiwan.

Institutional Review Board Statement: Not applicable.

Informed Consent Statement: Not applicable.

https://doi.org/10.3390/engproc2026159053

Data Availability Statement: The data presented in this study are available on request from the corresponding author.

Acknowledgments: The authors would like to thank Letizia Candia Villalba for her assistance with document formatting and proofreading during the final preparation of the manuscript.

Conflicts of Interest: The authors declare no conflicts of interest.

Abbreviations

The following abbreviations are used in this manuscript:

AOI	Automated Optical Inspection
PCB	Printed Circuit Board
PPP	Prismatic-Prismatic-Prismatic
ZV	Zero Vibration
ZVD	Zero Vibration and Derivative
FFT	Fast Fourier Transform
RMS	Root Mean Square

References

1. Mehmood, Y.; Cannella, F.; Cocuzza, S. Analytical Modeling, Virtual Prototyping, and Performance Optimization of Cartesian Robots: A Comprehensive Review. *Robotics* **2025**, *14*, 62. [CrossRef]
2. Jokinen, M. Centralized Motion Control of a Linear Tooth Belt Drive: Analysis of the Performance and Limitations. Ph.D. Dissertation, Acta Universitatis Lappeenrantaensis 407, Lappeenranta University of Technology, Lappeenranta, Finland, 26 November 2010. Available online: https://lutpub.lut.fi/handle/10024/66177 (accessed on 25 February 2026).
3. Singhose, W. Command Shaping for Flexible Systems: A Review of the First 50 Years. *Int. J. Precis. Eng. Manuf.* **2009**, *10*, 153–168. [CrossRef]
4. Singer, N.C.; Seering, W.P. Preshaping Command Inputs to Reduce System Vibration. *J. Dyn. Syst. Meas. Control* **1990**, *112*, 76–82. [CrossRef]
5. Meckl, P.H.; Seering, W.P. Experimental Evaluation of Shaped Inputs to Reduce Vibration for a Cartesian Robot. *J. Dyn. Syst. Meas. Control* **1990**, *112*, 159–165. [CrossRef]
6. Rao, S.S. *Mechanical Vibrations*, 6th ed.; Pearson: Hoboken, NJ, USA, 2018; pp. 317–320.
7. Singhose, W.E.; Derezinski, S.J.; Singer, N.C. Extra-Insensitive Input Shapers for Controlling Flexible Spacecraft. *J. Guid. Control Dyn.* **1996**, *19*, 385–391. [CrossRef] [PubMed]
8. Singhose, W.; Seering, W.; Singer, N. Input Shaping for Vibration Reduction with Specified Insensitivity to Modeling Errors. In *Proceedings of the 1996 Japan–USA Symposium on Flexible Automation, Boston, MA, USA, 7–10 July 1996*; ASME: New York, NY, USA, 1996; Volume 1, pp. 307–313.

Disclaimer/Publisher's Note: The statements, opinions and data contained in all publications are solely those of the individual author(s) and contributor(s) and not of MDPI and/or the editor(s). MDPI and/or the editor(s) disclaim responsibility for any injury to people or property resulting from any ideas, methods, instructions or products referred to in the content.